Mass transfer cavitation model with variable density of nuclei

A. Vallier*, H. Nilsson† and J. Revstedt*

* Division of Fluid Mechanics Dept. Energy Sciences, Lund University, SE-22100 Lund, Sweden

† Applied Mechanics, Fluid Dynamics, Chalmers University of Technology, SE-412 96 Gothenburg, Sweden

Aurelia.Vallier@energy.lth.se, hakan.nilsson@chalmers.se and Johan.Revstedt@energy.lth.se

Keywords: Cavitation, Sauer's model, Variable nuclei density, Lagrangian Particle Tracking

Abstract

The performance of the mass transfer cavitation model of Sauer is investigated using a varying nuclei concentration. The Sauer model assumes a uniform nuclei distribution despite measurement of the non-homogeneous nucleus population. Here the nuclei density is studied and a non-homogeneous nuclei distribution in a modified Sauer model is implemented. It is used to study how the increased cavitation nuclei density in regions of low pressure affects the inception of cavitation. The interface between the water and the water vapor is tracked using a volume of fluid method and vaporization and condensation are described by the modified Sauer's mass transfer model. The nuclei in the liquid phase are modeled with a Lagrangian Particle Tracking method. The LPT computations yield to a non uniform nuclei distribution which consists of nuclei accumulation close to the leading edge and no nuclei on average in the boundary layer of the hydrofoil. The sensitivity of the modified Sauer model to nuclei distribution is proven. The shape of the sheet cavity and the volume of vapour are affected by the nuclei content.

Nomenclature

Roman symbols

g	gravitational constant (ms^{-1})
p	pressure (Nm^{-2})
U	velocity (ms^{-1})
D	diameter (m)
R	radius (m)
c_0	chord length (m)
k	turbulent kinetic energy ($\mathrm{m}^2\mathrm{s}^{-2}$)

Greek symbols

α	vapor volume fraction
ρ	density (kgm^{-3})
μ	viscosity ($kgm^{-1}s^{-1}$)
τ	relaxation time (s)
ϵ	turbulence energy dissipation rate ($\mathrm{m}^2\mathrm{s}^{-3}$)

Subscripts

P	particle
v	vapor
l	liquid

Introduction

Recently, many mass transfer cavitation models have been introduced in the literature and general-purpose CFD codes in order to fully describe the observed phenomena on cavitating hydrofoils. The inception cavitation number is supposed to be given by the minimum value of the pressure coefficient. This law is barely suitable in the case of attached cavitation on a hydrofoil because viscosity, turbulence and water quality have a major influence on cavitation inception (Brennen (1995)). In particular, cavitation inception occurs at different pressure depending on the number of cavitation nuclei. Therefore, taking into account the non-homogeneous nuclei content of the water will improve the accuracy of the numerical simulations. Sauer (2000) included the nuclei density parameter n_0 in their cavitation model, specified as a constant . This assumption is not in accordance with experiments or the numerical results obtained by Huuva et al. (2007), where it is shown that the nuclei accumulate in certain regions close to the hydrofoil. Mass transfer models give very good predictions of the mechanism of the cavitation inception and development for cases of cavitating hydrofoils (Coutier-Delgosha et al. (2007)). These models successfully represent the attached sheet cavity, the re-entrant jet, the

break-off of the sheet, and the shedding of the break-off process. All these features agree with experimental observations. However, the models fail to resolve the transition between the attached sheet cavity and the cloud of vapor. In experiments, the transition forms a cloud of small vapor bubbles, while the numerical methods preserve a large coherent vapor region that is advected with the surrounding flow. The models cannot further handle the collapsing process of the small bubbles and the related erosive and acoustic processes. Indeed this important feature should at some point be included in the prediction as it is the main cause of erosion damage. The implosion of the bubble cloud when it reached a region of higher pressure generates pressure waves that influence the collapse of the surrounding bubbles, causing a chain reaction that amplifies the erosive process. As the model does not accurately predict regions containing a low vapor concentration, we study the relevance of the hypothesis made to simplify the model, i.e. the assumption of constant nuclei concentration. It is not obvious that the nuclei concentration is homogeneous in real application. Therefore it is of interest to investigate how a inhomogeneous distribution affects the inception and development of attached sheet cavities.

The Sauer cavitation mass transfer model is introduced with the nuclei density n_0, taking into account the water quality. Then the LPT method described is used to compute the cavitation nuclei distribution. Finally we present the results obtained for the LPT nuclei distribution and for the modified Sauer model where non homogeneity is included.

Geometry

The simulations were performed for 2D and 3D flows past a NACA0015 hydrofoil. Figure 1 illustrates the 125*270 C-grid used for the 2D computations. The hydrofoil has a chord length c_0=0.15m and is positioned at $4.5c_0$ from the inlet and $9c_0$ from the outlet. The height of the computational domain is $9c_0$. The angle of attack is 8 degrees. The grid points are clustered to the hydrofoil surface such that the first cell center near the hydrofoil surface starts at $\Delta y/c_0 \sim 0.1/\sqrt{Re} = 1.10^{-4}$ with an increase of 5% per layer. Hence, the first node away from the wall is on average positioned at $y^+ = 3$. In the case of the 3D simulation, 50 grid points are equally distributed in spanwise direction, with a total spanwise thickness of $1c_0$. The Reynolds number based on c_0 and the uniform inlet velocity 8m/s is Re=$1.2 \cdot 10^6$. The cavitation number σ is 1.2.

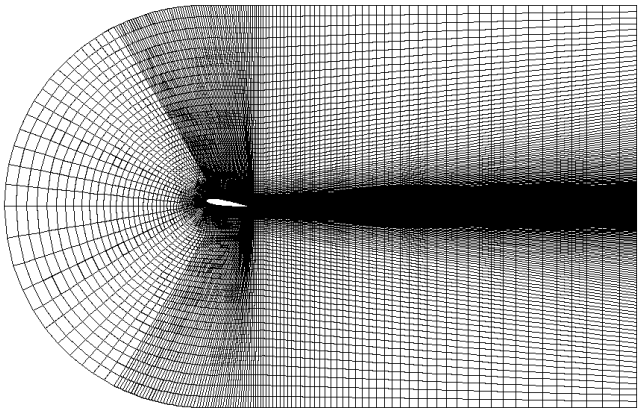

Figure 1: Computational grid for the NACA0015 airfoil

Sauer model

The Sauer model (Sauer (2000)) is a mass transfer model using the volume of fluid (VOF) approach. The fluid density and viscosity are scaled by the vapor volume fraction α

$$\rho = \alpha\rho_v + (1-\alpha)\rho_l \tag{1}$$

$$\mu = \alpha\mu_v + (1-\alpha)\mu_l \tag{2}$$

The transport equation for the vapor volume fraction reads

$$\frac{\partial\alpha}{\partial t} + \nabla\cdot(\alpha\mathbf{U}) = S_\alpha \tag{3}$$

where the source term $S_\alpha = -\frac{\dot{m}}{\rho_v}$ accounts for the destruction and production of vapor. One can also derive a corresponding transport equation for the liquid volume fraction γ (where $\alpha+\gamma=1$). The source term is then $S_\gamma = \frac{\dot{m}}{\rho_l}$ which accounts for the destruction and production of liquid. Summing the two transport equations results in the non divergence free continuity equation:

$$\nabla\cdot\mathbf{U} = (\frac{1}{\rho_l} - \frac{1}{\rho_l})\dot{m}$$

In order to derive the mass transfer rate, $\dot{m}$, the Sauer model states that the vapor volume fraction corresponds to a density n_0 of nuclei of radius R. Furthermore the dynamics of each bubble is governed by a simplified Rayleigh-Plesset equation. Hence the vapor volume fraction and the nuclei growth rate are written as

$$\alpha = \frac{\frac{4}{3}\pi R^3 n_0}{1+\frac{4}{3}\pi R^3 n_0} \tag{4}$$

$$\dot{R} = \sqrt{\frac{2}{3}\frac{|p(R) - p_\infty|}{\rho_l}}. \quad (5)$$

The mass transfer rate $\dot{m}$ is then derived (see Sauer (2000)) as

$$\dot{m} = -\rho_v \frac{3\alpha}{R} sign(p_v - p)\sqrt{\frac{2}{3}\frac{|p_v - p|}{\rho_l}} \quad (6)$$

Finally, the continuity and vapor transport equations are solved together with the momentum equation:

$$\rho\frac{\partial \mathbf{U}}{\partial t} + \rho(\mathbf{U}\cdot\nabla\mathbf{U}) = -\nabla p + \mu\nabla^2\mathbf{U} + \rho g \quad (7)$$

Nuclei distribution

Lagrangian Particle Tracking

Lagrangian particle tracking (LPT) is a method to track individual particles (or bubbles) in a fluid flow. A particle P is defined by the position of its center, $\mathbf{x_P}$, its diameter, D_P, its velocity, $\mathbf{U_P}$ and its density, ρ_P.

The fluid phase is governed by the incompressible Navier-Stokes equations

$$\nabla\cdot\mathbf{U} = 0$$

$$\rho\frac{\partial \mathbf{U}}{\partial t} + \rho(\mathbf{U}\cdot\nabla\mathbf{U}) = -\nabla p + \mu\nabla^2\mathbf{U} + \rho g - \mathbf{S_P} \quad (8)$$

The additional source term in the momentum equation (8) is due to the influence of the particles on the flow. Here we consider the case of a dilute suspension ($\frac{\mathbf{x_{P_i}} - \mathbf{x_{P_j}}}{D_P} > 10$) with a volume fraction of particles lower than 10^{-6}. Hence the particles' effects on the flow and turbulence are negligible (see Elghobashi (1994)). This is usually denoted one-way coupling, i.e. the flow affects the particles but the particles don't affect the flow. Therefore the additional source term $\mathbf{S_P}$ in the momentum equation is neglected. As a consequence of the very low volume fraction of particles, inter-particle collisions are also neglected.

In a Lagrangian frame, each particle position vector $\mathbf{x_P}$ is calculated from the equation

$$\frac{d\mathbf{x_P}}{dt} = \mathbf{U_P} \quad (9)$$

and the motion of each particle is governed by Newton's second law:

$$m_p\frac{d\mathbf{U_P}}{dt} = \sum \mathbf{F}, \quad (10)$$

where the mass of each particle is $m_P = \frac{1}{6}\rho_P\pi D_P^3$.

In dilute flow, the dominant forces acting on the small particle is the drag from the fluid phase and the gravitational force:

$$\sum \mathbf{F} = \mathbf{F_D} + m_p\mathbf{g} \quad (11)$$

The particle Reynolds number is defined as

$$\mathrm{Re}_P = \frac{\rho_f D_p|\mathbf{U} - \mathbf{U_p}|}{\mu_f} \quad (12)$$

and the drag force can be expressed as

$$\mathbf{F_D} = -m_p\frac{\mathbf{U_p} - \mathbf{U}}{\tau_P} \quad (13)$$

The relaxation time τ_p of the particles is the time it takes for a particle to respond to changes in the local flow velocity

$$\tau_p = \frac{4}{3}\frac{\rho_p D_p}{\rho_f C_D|\mathbf{U} - \mathbf{U_p}|} \quad (14)$$

where the standard definition of the drag coefficient C_D for a spherical particle is given by Schiller and Naumann as

$$C_D = \begin{cases} \frac{24}{Re_p} & \text{if } \mathrm{Re}_p \le 0.1 \\ \frac{24}{Re_p}(1 + \frac{1}{6}Re_p^{2/3}) & \text{if } 0.1 \le Re_p \le 1000 \\ 0.44 & \text{if } \mathrm{Re}_p > 1000 \end{cases} \quad (15)$$

Since the fluid velocity $\mathbf{U}$, calculated in the Eulerian reference frame, is needed for the calculation of the drag force in the Lagrangian frame, it has to be interpolated to the position of the particle from the neighboring cells. The velocity at the particle position is denoted $\mathbf{U_{@P}}$.

Furthermore, each Eulerian time step is divided into a set of Lagrangian time steps that is specific to each particle. A Lagrangian time step is defined as the time it takes for the particle to leave the cell that it was occupying.

The velocity and position of a particle at the n-th Lagrangian time step Δt_n within an eulerian time step is evaluated as

$$\mathbf{U_p^{t+\sum_{i=1}^{n}\Delta t_i}} = \frac{\mathbf{U_P^{t+\sum_{i=1}^{n-1}\Delta t_i}} + \mathbf{U_{@P}^{t}}\frac{\Delta t_n}{\tau_p} + \mathbf{g}\Delta t_n}{1 + \frac{\Delta t_n}{\tau_p}} \quad (16)$$

$$\mathbf{x_p^{t+\sum_{i=1}^{n}\Delta t_i}} = \mathbf{x_p^{t+\sum_{i=1}^{n-1}\Delta t_i}} + \mathbf{U_P^{t+\sum_{i=1}^{n-1}\Delta t_i}}\Delta t_n \quad (17)$$

The collision of a particle with the wall is assumed to be inelastic. Hence, the velocities of the particle P before and after collision are written as

$$\mathbf{U}_P = U_P^n\mathbf{n} + U_P^t\mathbf{t} \quad (18)$$

$$\mathbf{U}_P^{'} = U_P^{n'}\mathbf{n} + U_P^{t'}\mathbf{t} \quad (19)$$

The unit vectors $\mathbf{n}$ and $\mathbf{t}$ are the normal and tangential to the wall, respectively. The normal and tangential components of the particle velocity after a collision with the wall are evaluated as

$$U_P^{n'} = -\epsilon_w U_P^n \quad (20)$$

$$U_P^{t'} = (1 - \mu_w)U_P^t \tag{21}$$

where $\epsilon_w \in [0, 1]$ and $\mu_w \in [0, 1]$) are the coefficient of restitution and friction of the wall.

Random Walk

In reality, small particles have a short relaxation time and respond quickly to the flow fluctuations. Turbulence diverts the particles from their trajectory and small particles are trapped in eddies for a certain period of time. Not accounting for this leads to that the particles will follow the stream lines of the mean flow. Here we use a random walk model (Gosman & Ioannides (1983)) to include the effect of turbulent dispersion of the particles, i.e. eddies are created randomly and affect the particle trajectory. In practice, a local fluctuating component is added to the particle velocity, i.e. $\mathbf{U}_P$ becomes $\tilde{\mathbf{U}}_P = \mathbf{U}_P + \mathbf{U}_P^{fluct}$. The local fluctuating velocity can be estimated by

$$\mathbf{U}_P^{fluct} = \psi\sqrt{\frac{2}{3}k} \tag{22}$$

where ψ is a random number generated from a Gaussian distribution of zero mean and variance 1 ($\psi \in N(0, 1)$) and $\sqrt{\frac{2}{3}k}$ is the local RMS fluid velocity fluctuations for isotropic turbulence. The eddy life time (t_e) and the time needed by the particle to traverse the eddy (transit time t_{tr}) are calculated as

$$t_e = \frac{C_\mu^{0.63}\frac{k^{1.5}}{\epsilon}}{|\mathbf{U}_P^{fluct}|} \tag{23}$$

$$t_{tr} = -\tau_P ln(1 - \frac{l_e}{\tau_P|\mathbf{U} - \tilde{\mathbf{U}}_P|}). \tag{24}$$

The random walk algorithm consists of evaluating $\mathbf{U}_P^{fluct}$ according to equation (22) and a random number ψ, calculating the characteristics times t_e and t_{tr} and keeping $\mathbf{U}_P^{fluct}$ constant during the interaction time $t_{int} = min(t_e, t_{tr})$.

Results

Nuclei density sensitivity to particle properties

Several cases (listed in Table 1) have been studied in order to investigate the sensitivity of the solution to particle diameter and particle density. Also, all these cases have been simulated both with and without the random walk model. Furthermore one 3D case was simulated with LES to see how the turbulence affects the particles distribution.

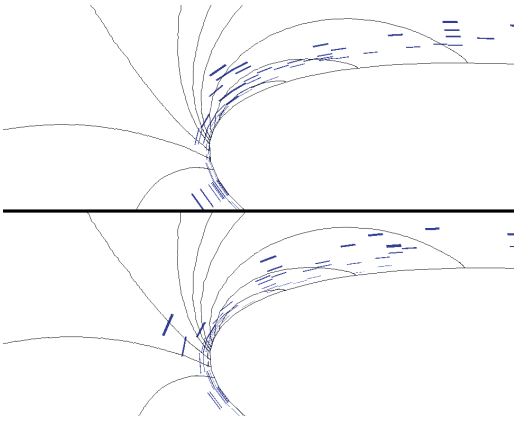

Figure 2: Instantaneous distribution of cells with a large nuclei density for cases $LPT6$ (top) and $LPT6_{RW}$ (bottom)

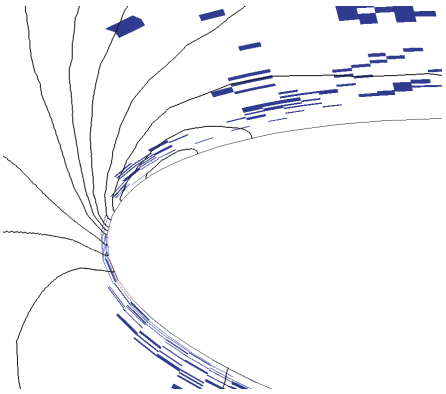

Figure 3: Instantaneous distribution of cells with a large nuclei density for case $LPT6_{LES}$, in the centerplane

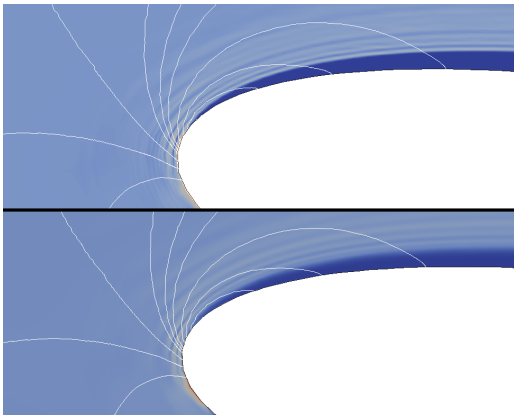

Figure 4: Average nuclei distribution for cases $LPT6$ and 6_{RW}

Table 1: Summary of the LPT cases.

ρ_P	D_P	2D RANS case name	2D RANS + RW case name	3D LES case name
1000	1	$LPT1$	$LPT1_{RW}$	
1000	10	$LPT2$	$LPT2_{RW}$	
1000	20	$LPT3$	$LPT3_{RW}$	
1000	30	$LPT4$	$LPT4_{RW}$	
1000	40	$LPT5$	$LPT5_{RW}$	
1000	50	$LPT6$	$LPT6_{RW}$	$LPT6_{LES}$
100	50	$LPT7$	$LPT7_{RW}$	
10	50	$LPT8$	$LPT8_{RW}$	
1	50	$LPT9$	$LPT9_{RW}$	

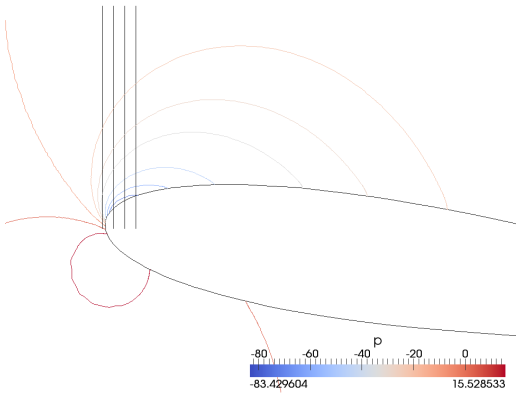

Figure 5: Contour of pressure (2D, RANS). Sampling lines where the average nuclei distribution is investigated.

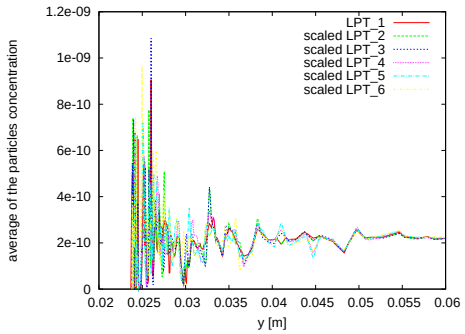

Figure 6: Sensitivity to particle size, sampling line 2

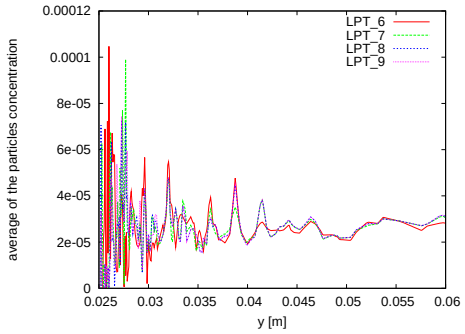

Figure 7: Sensitivity to particle density, sampling line 3

500 particles are injected per time step at a distance $1.5c_0$ in front of the hydrofoil.

Figures 2 and 3 highlight the cells which contain the largest number of nuclei for the RANS and LES computations. Two features are observed. First, a large number of nuclei are present at the leading edge. Obviously the density is highest at the stagnation point (colored in red) because the nuclei rebound against the wall and reside a longer time in this region of low velocity. Second, the presence of cells with a high nuclei content in the region of low pressure should be investigated. In this region the velocity is high and the residence time of a nuclei is therefore very short. From one instantaneous picture to another, the nuclei distribution is completely different. Thus we calculate an average of the positions occupied by the nuclei during their trajectory. Figure 4 shows the results for case $LPT6$ and $LPT6_{RW}$. The average nuclei distribution confirms the accumulation of nuclei at the stagnation point (colored in red) . A large number of nuclei are also observed in a part of the low pressure region near the leading edge. However the results show that the nuclei are not present on average in the boundary layer of the hydrofoil.

In order to compare the influence of the size and the density, as well as the turbulence modeling, the averaged nuclei distribution has been sampled on vertical lines through the low pressure region (Figure 5). In order to compare the nuclei density for different values of particle diameter D_P (case LPT1 to LPT6), the nuclei density is scaled and divided by $(D_P \cdot 10^6)^3$ in Figure 6. For all the cases, large fluctuations appear near the surface, followed by smaller fluctuations and then the nuclei density is almost constant and equal to the nuclei density injected. The size and density influence on the nuclei density is not important. The results are similar for each sampling line, therefore only one of them is presented here, in Figure 6 and 7. Near the surface the nuclei density reaches peak value up to five time the mean value but it also has very low values. This behavior is probably due to the very small size of the cells in this region. The interesting feature is the presence of the smaller fluctuations over the mean value which confirms that the concentration of nuclei is higher quite close to the surface.

The random walk model has an impact on the nuclei

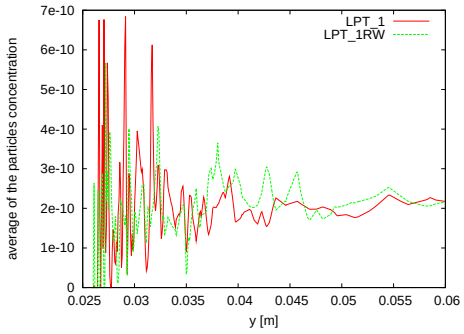

Figure 8: Sensitivity to Random Walk model, sampling line 4

distribution, as shown in Figure 8. The nuclei appear closer to the surface, the high fluctuations near the surface are reduced and the smaller fluctuations are translated upward. This means that a even higher nuclei density is predicted quite close to the surface.

Effect of inhomogeneous nuclei distribution

The Sauer model assumes a homogeneous nuclei distribution, and a value of 10^8 is generally used. Here the performance of the model is investigated using a varying nuclei concentration. Using the nuclei distributions obtained from the simulations presented in the previous section in the modified Sauer model did not yield any sheet cavitation. Instead, the cavity appeared somewhat above the hydrofoil and was not attached. Indeed the vapor production started where both crucial parameters existed, i.e. a low pressure and a high concentration of nuclei. This behavior is due to the lack of nuclei in the boundary layer discussed in the results of the LPT simulations. However, it has been shown experimentally that cavitation starts at the surface. This implies that the transported nuclei (called free stream nuclei) don't have as much importance as the surface nuclei, at least for cavitation inception. Surface nuclei are generally small bubble of gas trapped in wall rugosity (Brennen (1995)). Therefore it has also been studied how the nuclei content in the boundary layer affect cavitation inception and development.

In those studies it is assumed that the nuclei concentration N is high (N=10^8) in a layer attached to the surface and low (N=10^2 or N=10^4) everywhere else. The thickness of the layer δ_N varies from 0.5, 1,2 and 4 mm. The cases are summarized in Table 2.

Figure 9 shows the total volume of vapor in the entire computational domain during the cavitating process. In cases 1 and 5, the layer is 0.5 mm thick. The nuclei content is too low to enable the cavity to grow sufficiently. The production of vapor is lower during cavitation inception compare to the uniform case. In the other cases cavitation inception is similar to the case with uniform nuclei distribution. The same amount of vapor is created when the cavity grows. From t=0.02 s, the vapor production is slightly larger than in the uniform case. The cavity is broken by the reentrant jet, and from t=0.03 the vapor disappears at the same rate except for cases 2 and 3. For both cases, the volume of vapor decreases slower, grows again and then decreases as in the uniform case.

Table 2: Summary of the cases with a prescribed non uniform nuclei distribution. N is the nuclei concentration in the domain. δ_N is the thickness of the layer with high concentration of nuclei, i.e. where N=10^8.

	δ_N=0.5	δ_N=1	δ_N=2	δ_N=4
N=10^2	case 1	case 2	case 3	case 4
N=10^4	case 5	case 6	case 7	case 8

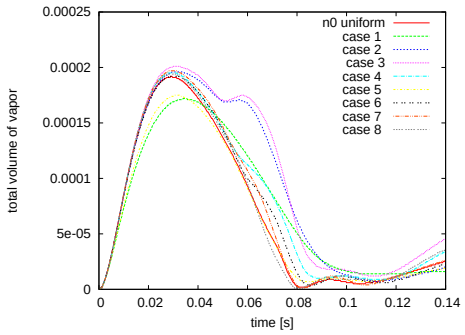

Figure 9: Total volume of vapor for cavitating flow with different nuclei distribution.

Figure 10 shows the cavitation process for the uniform case (left), case 7 (center) and case 3 (right). As mentioned, the inception is similar for all cases. The attached cavity has the same shape at t=0.02 s. Differences can be noticed from t=0.03 s, due to the re-entrant jet which has the same thickness as the layer of nuclei. For all the cases with $\delta_N \leq 2mm$ (here only $\delta_N = 2mm$ is shown) , the cloud which is about to be detached is closer to the hydrofoil surface. Furthermore the re-entrant jet is faster. Thus it breaks the attached cavity at a position closer to the leading edge. As the point of detachment is closer to the leading edge, the length of the attached cavity is shorter and the cloud is more stretched . With a non-uniform nuclei distribution, the attached cavity is linked to the cloud by a thin layer of vapor. This line of vapor is still present when the cloud shrinks (t=0.06). It generates a second smaller, fuzzier cloud for the cases with N=10^2. This is the reason why the total volume of vapor increases around t=0.06 s for these cases.

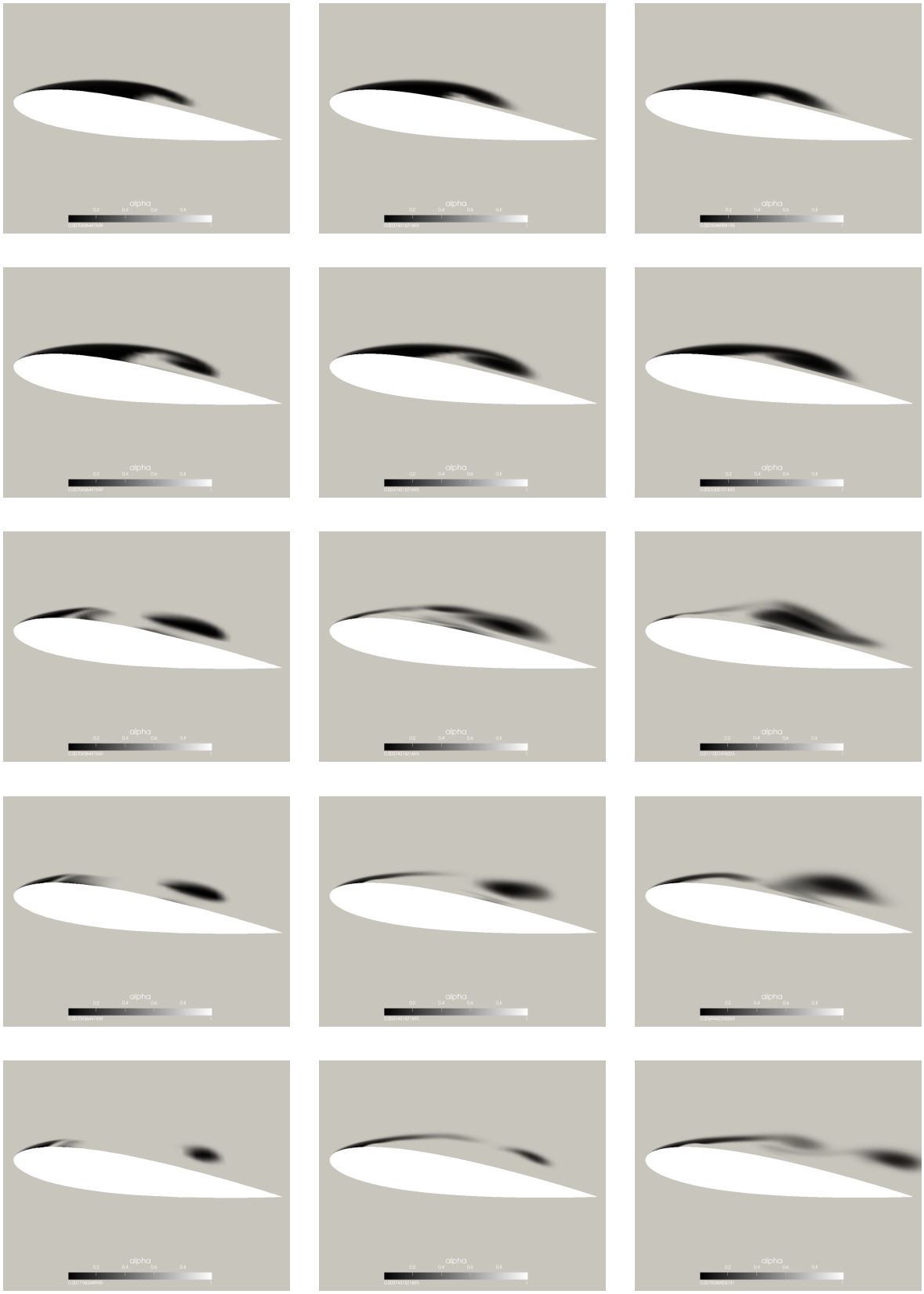

Figure 10: Vapor volume fraction α. First row t=0.02s, 2nd row t=0.03s, 3rd row t=0.05s, 4th row t=0.06s, 5th row t=0.07s. Left: N uniform, center: case 7 ($N = 10^4$, δ_N=2 mm), right: case 3 ($N = 10^2$, δ_N=2 mm)

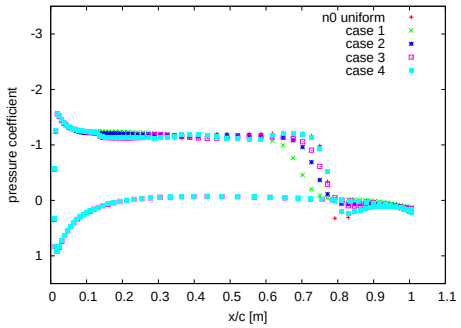

Figure 11: Pressure coefficient at t=0.03 s. Cases with N=10^2.

The differences between the curves of the pressure coefficient, shown in Figure 11, confirm that the non uniform cases have a shorter attached cavity already at t=0.03 as the the pressure increases at a position x/c_0 between=0.65 and 0.7 instead of 0.75 for the uniform case.

Conclusions

We studied the nuclei distribution over a NACA0015 hydrofoil. It was shown that the nuclei accumulate at the leading edge close to the low pressure region. However the nuclei were not present on average in the boundary layer. The Sauer model was modified to take into account this non uniform nuclei density and didn't yield to attached cavitation. It means that the transported nuclei influence is not as important as the one of the surface nuclei for cavitation inception. Then the performance of the modified Sauer model was investigated with a higher nuclei concentration near the surface. The attached cavity was shorter, the re-entrant jet was faster and thinner, and the cloud was stretched. A thin layer of vapor linked the attached cavity and the cloud of vapor. These features emphasize the importance of the nuclei distribution when modeling cavitation inception and developement.

Acknowledgements

The research presented was carried out as a part of "Swedish Hydropower Center - SVC". SVC has been established by the Swedish Energy Agency, Elforsk and Svenska Kraftnät together with Lulea University of Technology, The Royal Institute of Technology, Chalmers University of technology and Uppsala University. www.svc.nu.

We gratefully acknowledge the use of the computing resources of LUNARC, center for scientific and technical computing at Lund University. www.lunarc.lu.se.

References

Sauer J. and Schnerr G.H., Unsteady cavitating flow- A new cavitating model based on a modified front capturing method and bubble dynamics, Proceedings of 2000 ASME Fluid Engineering Summer Conference, Boston, MA, June 11-15, 2000

Huuva T., Cure A., Bark G. and Nilsson H., Computations of unsteady cavitating flow on wing profiles using a volume fraction method and mass transfer models. Proceedings of The 2nd IAHR International Meeting of the Workgroup on Cavitation and Dynamical Problems in Hydraulic Machinery and Systems, Scientific Bulletin of the "Polytechnica" University of Timisoara, Romania. Transactions on Mechanics, 52 (66) pp. 21-34, 2007

Coutier-Delgosha O., Deniset F., Astolfi J.A., Leroux J.-B., Numerical Prediction of cavitating Flw on a Two-Dimensional Symmetrical Hydrofoil and Comparison To Experiments, Journal of Fluids Engineering, march 2007, Vol. 129, 279-292.

Brennen C. E., Cavitation and Bubble Dynamics, New York Oxford University Press, 1995.

Clift R., Grace J.R and Weber M.E., Bubbles, Drops and Particles, Academic, New York,1978,

Gosman A.D. and Ioannides E., Aspects of computer simulation of liquid-fueled combustors, Journal of Energy,7, 482-490, 1983.

Elghobashi S., On predicting particle laden turbulent flows, Applied Scientific Research, 52, 309-329, 1994.